Relative timing of the ends of hurricane intensification and contraction of the radius of maximum wind in the North Atlantic and Eastern North Pacific

Yuanlong Li[1], Zhe-Min Tan[1*], Yuqing Wang[2]

[1]Key Laboratory of Mesoscale Severe Weather/MOE, and School of Atmospheric Sciences, Nanjing University, Nanjing, China

[2]International Pacific Research Center and Department of Atmospheric Sciences, School of Ocean and Earth Science and Technology, University of Hawaii at Manoa, Honolulu, Hawaii

June 19, 2022 (submitted)

August 26, 2022 (resubmitted)

October 12, 2022 (revised)

Dateline

Key Points:

- The end of contraction of the radius of maximum wind precedes the end of intensification in more than half of hurricanes.
- The preceding case occurs more readily in hurricanes with weaker intensity and larger curvature of inner-core tangential wind profile.
- The preceding time is longer in hurricanes with lower intensification rate and weaker intensity relative to maximum potential intensity.

Submitted to ***Geophysical Research Letters***

*Corresponding author address:

Zhe-Min Tan

School of Atmospheric Sciences, Nanjing University

163 Xianlin Avenue, Nanjing 210023, China

Email: zmtan@nju.edu.cn

Abstract: The statistical relationship between the ending times of hurricane intensification and contraction of the radius of maximum wind (RMW) over the North Atlantic (NA) and Eastern North Pacific (EP) is assessed using the Extended Best Track and Tropical Cyclone Observations-Based Structure databases during 1999–2014. Results show that in more than half of hurricanes the end of RMW contraction precedes the end of intensification, and those hurricanes generally have lower relative intensity (intensity normalized by the corresponding maximum potential intensity) and larger curvature of the tangential wind profile at the RMW. The preceding time tends to be longer with lower relative intensity and lower intensification rate and on average is longer in the NA (~19 h) than in the EP (~12 h) due to the overall lower intensification rate in the former. These findings can help improve our understanding of hurricane structure and intensity changes.

Plain language summary: It has been widely accepted that tropical cyclone (TC) intensification and contraction of the radius of maximum wind (RMW) often occur simultaneously. However, recent modelling and observational studies indicated that the contraction of RMW may terminate well before the end of intensification. By statistically analyzing the ending times of RMW contraction and intensification of TCs (with lifetime maximum intensity of category-1 hurricane or above) in the North Atlantic and Eastern North Pacific, we found that in more than half of hurricanes the end of RMW contraction precedes the end of intensification in both basins. The occurrence of this preceding phenomenon is critically related to the intensity and structure of TCs. The preceding time is determined by the TC intensification rate and intensity relative to the corresponding maximum theoretical intensity, both of which could be modified by environmental conditions. These findings provide a new perspective to improve the understanding and prediction of TC structure and intensity change.

1. Introduction

The link between changes in tropical cyclone (TC) intensity and the radius of maximum wind (RMW) has been an active topic of research on TC dynamics. Based on the balanced vortex dynamics (Eliassen, 1951), diabatic heating in the eyewall tends to yield a tangential wind tendency that is maximized inside the RMW, facilitating the contraction of the RMW (Shapiro & Willoughby, 1982). As a result, conceptually, TC intensification is generally believed to be coincident with RMW contraction (e.g., Willoughby, 1990; Holland, 1997; Hogsett & Stewart, 2014). However, several recent modelling and observational studies have found that RMW contraction may terminate well before the end of intensification (e.g., Kieu, 2012; Stern et al., 2015; Li et al., 2019). The statistical analyses of Qin et al. (2016) also showed that a quasi-steady state in the RMW often occurs during the later stages of TC rapid intensification of 24-h or 12-h durations, implying that intensification and RMW contraction do not necessarily occur simultaneously.

Using a novel diagnostic equation for RMW, Stern et al. (2015) ascribed the cessation of RMW contraction to the increased curvature of the tangential wind profile at the RMW, which has been further analyzed by Li et al. (2019). Morphologically, a larger curvature at the RMW implies a larger inward drop in tangential wind speed from the RMW, and thus to contract RMW, a greater negative gradient of tangential wind tendency inside the RMW is required. The theoretical framework of Stern et al. (2015) indicates that the cessation of RMW contraction may tend to precede the end of intensification because the curvature of the tangential wind profile generally increases rapidly as a TC intensifies and RMW contracts (Stern et al., 2015; Li et al., 2019) , which limits the RMW contraction.

TC intensity prediction is known to be challenging in operational TC forecasting (DeMaria et al., 2014). An important and difficult challenge for TC intensity forecasting is the timing of lifetime maximum intensity (i.e., the end of intensification), which affects the TC evolution in the subsequent landfall or weakening stage (Fei et al., 2020). Although the maximum potential intensity (MPI) theory may give a reference for the prediction of lifetime maximum intensity, most TCs cannot achieve their MPI in nature (Emanuel, 1999, 2000). Therefore, if the end of RMW contraction precedes the end of intensification in nature as implied by the theoretical work of Stern et al. (2015) and the preceding time can be estimated, the ending time of contraction may provide a new perspective to predict the timing of lifetime maximum intensity of a TC.

The objective of the present study is to test the aforementioned hypothesis via systematically analyzing the climatology of the relative timing of ends of intensification and RMW contraction of TCs in the North Atlantic (NA) and Eastern North Pacific (EP). We will answer the following questions: (1) Does the end of contraction generally precede the end of intensification in nature, and if so, how frequently and on average how long the end of contraction precedes the end of intensification? (2) What potentially affects the preceding time? and (3) Is there any inter-basin difference in the relative timing, and if so, what causes the difference?

2. Data and methods

2.1. TC data

The Extend Best Track (EBT) dataset (Demuth et al., 2006) of version 3.0.0 is used to obtain intensity and wind structure information for TCs over the NA and EP. To ensure the robustness of our results, the NA Tropical Cyclone Observations-Based Structure (TC-OBS) dataset (Vigh et al., 2016) of version 0.40 is also used. Both datasets contain the TC location, intensity in terms of maximum sustained 10-m wind speed (*Vmax*), RMW, eye size, radii of 17.5 m s^{-1} (R175), distance to the nearest major landmass, and an indicator of whether the system is purely tropical, subtropical, or extra-tropical. The years of 1999–2014 are used with six-hourly intervals for both datesets because the RMW data in EBT are of better quality from 1999 with the use of the Advanced Microwave Sounding Unit data (Demuth et al., 2004; Wu & Ruan, 2021), and the TC-OBS dataset ends at 2014. Note that in both datasets the RMWs are not "best tracked". To further ensure the robustness of our results, as in Davis (2018) and Chavas & Knaff (2022), additional analysis (lablled as ER11) is also performed for both basins as with EBT but using an objectively computed RMWs based on the inner-core wind structure model of Emanuel & Rotunno (2011). The model equation is

$$\left(\frac{M}{M_{\mathrm{RMW}}}\right)^{2-(C_k/C_D)} = \frac{2(r/\mathrm{RMW})^2}{2-(C_k/C_D)+(C_k/C_D)(r/\mathrm{RMW})^2}, \quad (1)$$

where M is the absolute angular momentum [$M = rV + (1/2)fr^2$, V is the tangential wind speed, r is radius from the TC center, and f is the Coriolis parameter at the TC center], C_k and C_D are the surface exchange coefficient and drag coefficient, respectively, and C_k/C_D is typically in the range of [0.4,1] in nature (Chavas et al., 2015). A complete evaluation of the model (Eq. 1) using observations can be found in Chavas et al. (2015). Namely, with the best tracked *Vmax* and R175 from EBT and assuming that $C_k/C_D = 0.9$ and *Vmax* is approximately equal to the maximum tangential wind (Li et al. 2020), RMW can be obtained by numerically solving Eq. (1).

For each of the analyses based on EBT, TC-OBS, and ER11, several objective criteria are used to obtain available TCs as follows: (1) TCs whose lifetime maximum intensity is weaker than 33 m s^{-1} (category-1 hurricane) are removed; (2) as a quality check following Kimball & Mulekar (2004) and Kossin et al. (2007), those records with RMW smaller than the radius of eye, or with *Vmax* greater than 17.5 m s^{-1} but RMW greater than R175 are removed; (3) those records with distance to the nearest major landmass less than 100 km are removed; (4) those records that are identified as subtropical or extra-tropical systems are removed; (5) Only the longest consecutive records for each TC is retained, and TCs with less than four valid records are removed; (6) TCs with RMW expansion greater than 30 km in 6 h before the ending time of intensification or contraction are removed to reduce the effect of concentric eyewall replacement on the results (Sitkowski et al., 2011). The ending time of intensification (contraction) is defined as the first time when intensity (RMW) attains the lifetime maximum intensity (minimum RMW).

2.2. Environmental factors

The potential impacts of large-scale environmental conditions on the relative timing of ends of intensification and contraction are investigated based on the 0.75° resolution European Centre for Medium-Range Weather Forecasts interim reanalysis data (ERA-Interim; Dee et al., 2011). The two known major environmental factors affecting TC evolution, i.e., the MPI and vertical wind shear (Emanuel, 1999; Tang & Emanuel, 2012), are examined. The MPI describes the upper bound of the intensity that a TC can achieve under given favorable thermodynamic conditions and is calculated by (Bister & Emanuel, 2002),

$$\mathrm{MPI} = \alpha\sqrt{\frac{C_k}{C_D}\frac{T_s}{T_0}(CAPE^* - CAPE)|_{\mathrm{RMW}}}, \tag{2}$$

where α is the reduction factor of gradient wind to 10-m wind, T_s is the sea surface temperature, and T_0 is the outflow-layer air temperature. $CAPE^*$ is the convective available potential energy with air parcel lifted from saturation at the sea surface, and $CAPE$ is that from the boundary layer, both are defined at the RMW of the hypothetical TC. The MPI calculation follows the code obtained from ftp://texmex.mit.edu/pub/emanuel/TCMAX/, with α and C_k/C_D set to 0.8 and 0.9 by default, and T_s, T_0, and atmospheric sounding in calculating $CAPE^*$ and $CAPE$ defined as the average within a radius of two times the RMW from the TC center. Vertical wind shear is defined as the difference of vector winds between 200–850 hPa averaged within a radius of 300 km from the TC center, with the disturbances in wind fields with wavelengths less than 1000 km removed (Kurihara et al., 1993).

3. Results

3.1. The relative timing

Since the results are qualitatively consistent in the NA and EP, we first focus on the NA. The percentages of TCs with the end of contraction preceding (PRE), occurring simultaneously with (SIM), and lagging (LAG) the end of intensification are ~60%, ~20%, and ~20%, respectively, based on EBT and TC-OBS (Fig. 1a). They are referred to as preceding, simultaneous, and lagging cases hereafter. The analysis based on ER11 also shows that the majority of TCs are the preceding cases (Fig. 1a), and the percentage of simultaneous case is higher in ER11 than in EBT and TC-OBS. The differences in the timing between the ends of intensification and contraction are greater than zero in more than ~70% of TCs in all three analyses (Fig. 1b). On average, the end of contraction precedes the end of intensification by ~19 h (Fig. 1b). The composites of *Vmax* and RMW based on the ending time of contraction also show the end of contraction preceding the end of intensification in all three analyses (Figs. 1c–e). Overall, despite with some quantitative differences, results in all three analyses are qualitatively consistent. Namely, the end of contraction predominantly precedes the end of intensification, supporting the theoretical implication from Stern et al. (2015). We also pick out those EBT records with aircraft observations based on f-deck file (a file that contains records of the fixes of storms; https://ftp.nhc.noaa.gov/atcf/archive/), and find that the composite result is similar to that with all EBT records (Figs. 1c,f). This further confirms the robustness of our main conclusion.

3.2. Differences in TC characteristics

It is our interest to address the key structure features that explain the relative timing of ends of intensification and contraction. Figure 2 compares the characteristics of TCs in the three cases at the time when the preceding cases (and simultaneous cases) and lagging cases (and simultaneous cases) end their contraction and intensification, respectively (cf. Fig. 2a). The simultaneous and lagging cases show stronger intensities (~45 m s^{-1} on average) at the ending time of intensification than the preceding cases (~35 m s^{-1} on average) at the ending time of contraction (Fig. 2b). We also compare the relative intensity, defined as the TC intensity normalized by its average MPI, for the three cases in Fig. 2c. Obviously, the simultaneous and lagging cases show a higher relative intensity (~0.75 on average) at the ending time of intensification than the preceding cases (~0.55 on average) at the ending time of contraction. This is consistent with previous findings that TCs with weaker intensity have a higher potential to experience intensification (Kaplan & DeMaria, 2003; Xu & Wang, 2015, 2018).

The preceding and simultaneous cases show a smaller RMW (~32 km on average) at the ending time of contraction than the lagging cases (~45 km on average) at the ending time of intensification (Fig. 2d). This is consistent with previous statistical studies by Wu & Ruan (2021) and Li et al. (2022), who found that larger RMW generally has higher potential to contract. As mentioned earlier, the RMW contraction rate decreases with the increasing curvature of the tangential wind profile at the RMW (Stern et al., 2015), defined as

$$C = -\frac{\partial^2 V}{\partial r^2}|_{\mathrm{RMW}}. \tag{3}$$

We estimate the curvature of the three cases with the wind profile near the RMW calculated by Eq. (1) for the given *Vmax* and RMW in all three analyses, with the results shown in Fig. 2e ($C_k/C_D = 1$) and Fig. 2f ($C_k/C_D = 0.5$). As shown in Chavas et al. (2015), a higher C_k/C_D tends to yield a larger curvature. Nevertheless, the overall results for the two assumed C_k/C_D are qualitatively consistent, i.e., as expected, the preceding and simultaneous cases at the ending time of contraction show a larger (~1.5–2 times) curvature than the lagging cases at the ending time of intensification. Note that the larger curvature in the former is associated with its smaller RMW (Fig. 2d; Stern et al., 2015).

The above results indicate that the relative timing of ends of intensification and contraction depends largely on TC's characteristics. Intensification tends to continue (terminate) with low (high) relative intensity, and RMW contraction tends to continue (stop) with small (large) curvature of tangential wind profile near the RMW. Therefore, the preceding, simultaneous, and lagging cases tend to occur when TCs are at relatively low relative intensity with large curvature, high relative intensity with large curvature, and high relative intensity with small curvature, respectively.

3.3. Preceding time

As shown in Fig. 1b, the preceding time shows large variability as also noticed by Stern et al. (2015). A question arises as to what determines the preceding time. There is a general negative (positive) correlation between the non-negative preceding time and average TC intensity (RMW) between the ending times of contraction and intensification in all three analyses (Figs. 3a,b). This is because both stronger intensity and smaller RMW imply a higher inner-core inertial stability, which can be approximated by the ratio of TC intensity to RMW (Li et al., 2021; Fig. 3c), and thus a higher dynamical efficiency in spinning up the TC inner core by eyewall heating (Schubert & Hack, 1982; Vigh & Schubert, 2009). A higher intensification rate will make the TC reaching its maximum intensity earlier and thus shorten the preceding time. As depicted in Fig. 3d, a significant (i.e., at the 95% confidence level under the student's *t*-test) negative correlation can be found between the preceding time and intensification rate.

In addition, a stronger TC intensity generally corresponds to higher relative intensity and a lower potential for a TC to intensify further, and thus a shorter preceding time (Fig. 3e). Nevertheless, there is no significant correlation between the preceding time and MPI in all three analyses (Fig. 3f). This is because on one hand a higher MPI implies a lower relative intensity, which tends to lengthen the preceding time (Fig. 3e), and on the other hand, it implies a condition more favorable for increasing intensification rate (Emanuel, 2012; Wang et al., 2021a,b), which tends to shorten the preceding time (Fig. 3d).

The preceding time tends to be longer with stronger vertical wind shear (Fig. 3g). This is because vertical wind shear is one of the key factors that is negative to TC intensification rate (Kaplan & DeMaria, 2003; Tang & Emanuel, 2012). In addition, the preceding time tends to be shorter for TCs with a shorter distance to the nearest major landmass (Fig. 3h). This is probably because TC intensification is often halted by large landmass if a TC is close to the coastline (Wu et al, 2009; Kaplan et al., 2010). This means that the preceding time is not necessarily longer under a more detrimental condition. Considering both intensification rate and relative intensity could be modified by environmental conditions, future refinements are needed to further examine/quantify the effect of environmental factors on the preceding time.

3.4. Inter-basin difference

Although the results are qualitatively consistent in the NA and EP (Fig. 1,4; Figs 2–3 and Supplementary Figs. S1–S2), the overall time difference between the ends of contraction and intensification is longer in the NA than in the EP for both EBT and ER11 analyses (Fig. 4b; Figs. 1c,e and Figs 4c,d). On average, the preceding time is ~19 h in the NA and ~12 h in the EP (Fig. 4b). Since the time difference is primarily contributed by the preceding cases (Supplementary Fig. S3), only the inter-basin differences in the preceding cases are examined. Results in Fig. 3 (and Supplementary Fig. S2) have shown that the preceding time is largely controlled by the relative intensity and intensification rate between the ending times of contraction and intensification. Since the (relative) intensity at the end of contraction partly depends on the intensification rate prior to this time, we compare both the average intensification rates prior to and after (but no later than the end of intensification) the end of contraction between the two basins in Fig. 4e (based on EBT). Significant differences are found in the two periods, and the overall intensification rates are higher in the EP than in the NA, consistent with previous statistical studies (Kaplan et al., 2010; Li et al., 2022). The higher intensification rate after the end of contraction could make the TC attaining its maximum intensity earlier and shorten the preceding time directly (Fig. 3d). The higher intensification rate prior to the end of contraction could partly induce the higher TC intensity and thus higher relative intensity (Fig. 4f), which could also contribute to the shorter preceding time in the EP (cf. Fig. 3e).

Therefore, we can conclude that the shorter preceding time in the EP is associated with the overall higher intensification rate, which is probably due to the more favorable environmental conditions, such as the higher sea surface temperature (thus higher MPI) and weaker vertical wind shear (Figs. 4g–i), in the EP than in the NA as suggested by Kaplan et al. (2010). The difference in the average MPI after the end of contraction is not as significant as that prior to this time (Fig. 4g), which is consistent with the greater sea surface temperature gradient along the TC track in the EP than in the NA (Fig. 4i, Foltz et al., 2018).

4. Conclusions and discussions

By analyzing the statistical relationship between the ending times of intensification and contraction for NA and EP hurricanes during 1999–2014, we show that in more than half of hurricanes the end of contraction precedes the end of intensification in both basins. The preceding case occur more readily in TCs with lower relative intensity and larger curvature of tangential wind profile at the RMW, and the preceding time tends to be longer for TCs with lower relative intensity and lower intensification rate. In both basins, in more than ~90% of hurricanes the non-negative preceding time is lower than 48 h as the relative intensity (intensification rate) greater than ~0.85 (13 m s^{-1} day^{-1}). On average, the preceding time is longer in the NA (~19 h) than in the EP (~12 h), consistent with the overall lower intensification rate in the former. Note that this study focuses only on intense TCs (i.e., hurricanes), and the percentage of preceding case would be reduced for weak TCs (Supplementary Fig. S5), because the intensification of weak TCs is more likely to be affected by detrimental environmental dynamical processes (Stern et al., 2015).

Although the RMW data are not "best tracked" for all three analyses, the results are qualitatively consistent. It could be a topic for a future work to further verify and quantify the relationship between the ends of contraction and intensification when more reliable data are available. Results from this study provide a new perspective to help improve the understanding and prediction of the timing of lifetime maximum intensity based on the timing of lifetime minimum RMW (or the end of contraction) in the future. Unlike maximum intensity, less studies have focused on the minimum RMW in the literature and there is no complete theoretical framework for the minimum RMW to date. As the first step, our major interest has been to examine the relationship between the ending times of contraction and intensification, and our findings suggest that more studies should be conducted to understand the minimum RMW based on theory, numerical simulations, and observational analysis in the near future.

Acknowledgments.

The authors thank three anonymous reviewers for their constructive review comments. This study was supported by National Natural Science Foundation of China under grants 42205001, 42192555, and 41730960 and the National Key R&D Program of China under grant 2017YFC1501602 and in part by

NSF grant AGS-1834300. Y. Li is also supported by China Postdoctoral Science Foundation (BX2021121; 2021M700066) and the Fundamental Research Funds for the Central Universities (020714380185).

Open Research

The EBT data are summarized in Demuth et al. (2006) and freely available at https://rammb2.cira.colostate.edu/research/tropical-cyclones/tc_extended_best_track_dataset/. The TC-OBS data are summarized in Vigh et al. (2016) and freely available at https://verif.rap.ucar.edu/tcdata/historical/database/. The ERA-Interim data are summarized in Dee et al. (2011) and freely available at https://apps.ecmwf.int/datasets/data/interim-full-daily/levtype=pl/.

References

Bister, M., & Emanuel, K. A. (2002), Low frequency variability of tropical cyclone potential intensity 1. Interannual to interdecadal variability. *Journal of Geophysical Research: Atmospheres*, *107*(D24), ACL-26, doi:10.1029/2001JD000776.

Chavas, D. R., & Knaff, J. A. (2022), A simple model for predicting the tropical cyclone radius of maximum wind from outer size. *Weather and Forecasting*, *37*(5), 563-579, doi:10.1175/WAF-D-21-0103.1.

Chavas, D. R., Lin, N., & Emanuel, K. (2015), A model for the complete radial structure of the tropical cyclone wind field. Part I: Comparison with observed structure. *Journal of the Atmospheric Sciences*, *72*(9), 3647–3662, doi:10.1175/JAS-D-15-0014.1.

Davis, C. A. (2018). Resolving tropical cyclone intensity in models. *Geophysical Research Letters*, *45*(4), 2082–2087. https:// doi.org/10.1002/2017GL076966.

Dee, D. P., Uppala, S. M., Simmons, A. J., Berrisford, P., Poli, P., Kobayashi, S., ... & Vitart, F. (2011), The ERA-Interim reanalysis: Configuration and performance of the data assimilation system. *Quarterly Journal of the royal meteorological society*, *137*(656), 553–597, doi:10.1002/qj.828.

DeMaria, M., Sampson, C. R., Knaff, J. A., & Musgrave, K. D. (2014), Is tropical cyclone intensity guidance improving? *Bulletin of the American Meteorological Society*, *95*(3), 387–398, doi:10.1175/BAMS-D-12-00240.1.

Demuth, J. L., DeMaria, M., Knaff, J. A., & Vonder Haar, T. H. (2004), Evaluation of Advanced Microwave Sounding Unit tropical-cyclone intensity and size estimation algorithms. *Journal of Applied Meteorology*, *43*(2), 282–296, doi:10.1175/1520-0450(2004)043%3C0282: EOAMSU%3E2.0.CO;2.

Demuth, J. L., DeMaria, M., & Knaff, J. A. (2006). Improvement of Advanced Microwave Sounding Unit tropical cyclone intensity and size estimation algorithms. *Journal of applied meteorology and climatology*, *45*(11), 1573–1581, doi:10.1175/JAM2429.1.

Eliassen, A. (1951), Slow thermally or frictionally controlled meridional circulation in a circular vortex. *Astrophysica Norvegica*, *5*, 19.

Emanuel, K. A. (1999), Thermodynamic control of hurricane intensity. *Nature*, *401*(6754), 665–669, doi:10.1038/44326.

Emanuel, K. (2000), A statistical analysis of tropical cyclone intensity. *Monthly weather review*, *128*(4), 1139–1152, doi:10.1175/1520-0493(2000)128%3C1139:ASAOTC%3E2.0.CO;2.

Emanuel, K., & Rotunno, R. (2011), Self-stratification of tropical cyclone outflow. Part I: Implications for storm structure. *Journal of the Atmospheric Sciences*, *68*(10), 2236–2249. doi:10.1175/JAS-D-10-05024.1.

Emanuel, K. (2012), Self-stratification of tropical cyclone outflow. Part II: Implications for storm intensification. *Journal of the atmospheric sciences*, *69*(3), 988–996, doi:10.1175/JAS-D-11-0177.1.

Fei, R., Xu, J., Wang, Y., & Yang, C. (2020), Factors affecting the weakening rate of tropical cyclones over the western north pacific. *Monthly Weather Review*, *148*(9), 3693–3712, doi:10.1175/MWR-D-19-0356.1.

Foltz, G. R., Balaguru, K., & Hagos, S. (2018), Interbasin differences in the relationship between SST and tropical cyclone intensification. *Monthly Weather Review*, *146*(3), 853–870, doi:10.1175/MWR-D-17-0155.1.

Hogsett, W. A., & Stewart, S. R. (2014), Dynamics of tropical cyclone intensification: Deep convective cyclonic "left movers". *Journal of the Atmospheric Sciences*, *71*(1), 226–242, doi:10.1175/JAS-D-12-0284.1.

Holland, G. J. (1997), The maximum potential intensity of tropical cyclones. *Journal of the atmospheric sciences*, *54*(21), 2519–2541, doi:10.1175/1520-0469(1997)054%3C2519:TMPIOT%3E2.0.CO;2.

Kaplan, J., & DeMaria, M. (2003), Large-scale characteristics of rapidly intensifying tropical cyclones in the North Atlantic basin. *Weather and forecasting*, *18*(6), 1093–1108, doi:10.1175/1520-0434(2003)018%3C1093:LCORIT%3E2.0.CO;2.

Kaplan, J., DeMaria, M., & Knaff, J. A. (2010), A revised tropical cyclone rapid intensification index for the Atlantic and eastern North Pacific basins. *Weather and forecasting*, *25*(1), 220–241, doi:10.1175/2009WAF2222280.1.

Kieu, C. Q. (2012), An investigation into the contraction of the hurricane radius of maximum wind. *Meteorology and Atmospheric Physics*, *115*(1), 47–56, doi:10.1007/s00703-011-0171-7.

Kimball, S. K., & Mulekar, M. S. (2004), A 15-year climatology of North Atlantic tropical cyclones. Part I: Size parameters. *Journal of Climate*, *17*(18), 3555–3575, doi:10.1175/1520-0442(2004)017%3C3555:AYCONA%3E2.0.CO;2.

Kossin, J. P., Knaff, J. A., Berger, H. I., Herndon, D. C., Cram, T. A., Velden, C. S., ... & Hawkins, J. D. (2007), Estimating hurricane wind structure in the absence of aircraft reconnaissance. *Weather and Forecasting*, *22*(1), 89–101, doi:10.1175/WAF985.1.

Kurihara, Y., Bender, M. A., & Ross, R. J. (1993), An initialization scheme of hurricane models by vortex specification. *Monthly weather review*, *121*(7), 2030–2045, doi:10.1175/1520-0493(1993)121<2030:AISOHM>2.0.CO;2.

Li, Y., Wang, Y., & Lin, Y. (2019), Revisiting the dynamics of eyewall contraction of tropical cyclones. *Journal of the Atmospheric Sciences*, *76*(10), 3229–3245, doi:10.1175/JAS-D-19-0076.1.

Li, Y., Wang, Y., & Lin, Y. (2020), How much does the upward advection of the supergradient component of boundary layer wind contribute to tropical cyclone intensification and maximum intensity? *Journal of the Atmospheric Sciences*, *77*(8), 2649–2664, doi:10.1175/JAS-D-19-0350.1.

Li, Y., Wang, Y., Lin, Y., & Wang, X. (2021), Why does rapid contraction of the radius of maximum wind precede rapid intensification in tropical cyclones? *Journal of the Atmospheric Sciences*, *78*(11), 3441–3453, doi:10.1175/JAS-D-21-0129.1.

Li, Y., Wang, Y., & Tan, Z.-M. (2022), How frequently does rapid intensification occur after rapid contraction of the radius of maximum wind in tropical cyclones over the North Atlantic and Eastern North Pacific? *Monthly Weather Review*, doi:10.1175/MWR-D-21-0322.1.

Qin, N., Zhang, D.-L., & Li, Y. (2016), A statistical analysis of steady eyewall sizes associated with rapidly intensifying hurricanes. *Weather and Forecasting*, *31*(3), 737–743, doi:10.1175/WAF-D-16-0016.1.

Shapiro, L. J., & Willoughby, H. E. (1982), The response of balanced hurricanes to local sources of heat and momentum. *Journal of the Atmospheric Sciences*, *39*(2), 378–394, doi:10.1175/1520-0469(1982)039%3C0378:TROBHT%3E2.0.CO;2.

Schubert, W. H., & Hack, J. J. (1982), Inertial stability and tropical cyclone development. *Journal of the Atmospheric Sciences*, *39*(8), 1687–1697, doi:10.1175/1520-0469(1982)039%3C1687:ISATCD%3E2.0.CO;2.

Sitkowski, M., Kossin, J. P., & Rozoff, C. M. (2011), Intensity and structure changes during hurricane eyewall replacement cycles. *Monthly Weather Review*, *139*(12), 3829-3847, doi:10.1175/MWR-D-11-00034.1.

Stern, D. P., Vigh, J. L., Nolan, D. S., & Zhang, F. (2015), Revisiting the relationship between eyewall contraction and intensification. *Journal of the Atmospheric Sciences*, *72*(4), 1283–1306, doi:10.1175/JAS-D-14-0261.1.

Vigh, J. L., & Schubert, W. H. (2009), Rapid development of the tropical cyclone warm core. *Journal of the Atmospheric Sciences*, *66*(11), 3335–3350, doi:10.1175/2009JAS3092.1.

Vigh, J. L., Gilleland, E., Williams, C. L., Chavas, D. R., Dorst, N. M., Done, J., Holland, G., & Brown, B. G. (2016), A new historical database of tropical cyclone position, intensity, and size parameters optimized for wind risk modeling. *32nd Conf. on Hurricanes and Tropical Meteorology, San Juan, Puerto Rico, Amer. Meteor. Soc., 12C.2*, doi:10.13140/RG.2.1.3720.5361.

Wang, Y., Li, Y., & Xu, J. (2021a), A new time-dependent theory of tropical cyclone intensification. *Journal of the Atmospheric Sciences*, *78*(12), 3855–3865, doi:10.1175/JAS-D-21-0169.1

Wang, Y., Li, Y., Xu, J., Tan, Z. M., & Lin, Y. (2021b), The intensity dependence of tropical cyclone intensification rate in a simplified energetically based dynamical system model. *Journal of the Atmospheric Sciences*, *78*(7), 2033–2045, doi:10.1175/JAS-D-20-0393.1.

Willoughby, H. E. (1990), Temporal changes of the primary circulation in tropical cyclones. *Journal of Atmospheric Sciences*, *47*(2), 242–264, doi:10.1175/1520-0469(1990)047%3C0242:TCOTPC%3E2.0.CO;2.

Wu, C. C., Cheng, H. J., Wang, Y., & Chou, K. H. (2009), A numerical investigation of the eyewall evolution in a landfalling typhoon. *Monthly weather review*, *137*(1), 21–40, doi:10.1175/2008MWR2516.1.

Wu, Q., & Ruan, Z. (2021), Rapid contraction of the radius of maximum tangential wind and rapid intensification of a tropical cyclone. *Journal of Geophysical Research: Atmospheres*, *126*(3), e2020JD033681, doi:10.1029/2020JD033681.

Xu, J., & Wang, Y. (2015), A statistical analysis on the dependence of tropical cyclone intensification rate on the storm intensity and size in the North Atlantic. *Weather and Forecasting*, *30*(3), 692–701, doi:10.1175/WAF-D-14-00141.1.

Xu, J., & Wang, Y. (2018), Dependence of tropical cyclone intensification rate on sea surface temperature, storm intensity and size in the western North Pacific. *Weather and Forecasting*, *33(2)*, 523–537, doi:10.1175/WAF-D-17-0095.1.

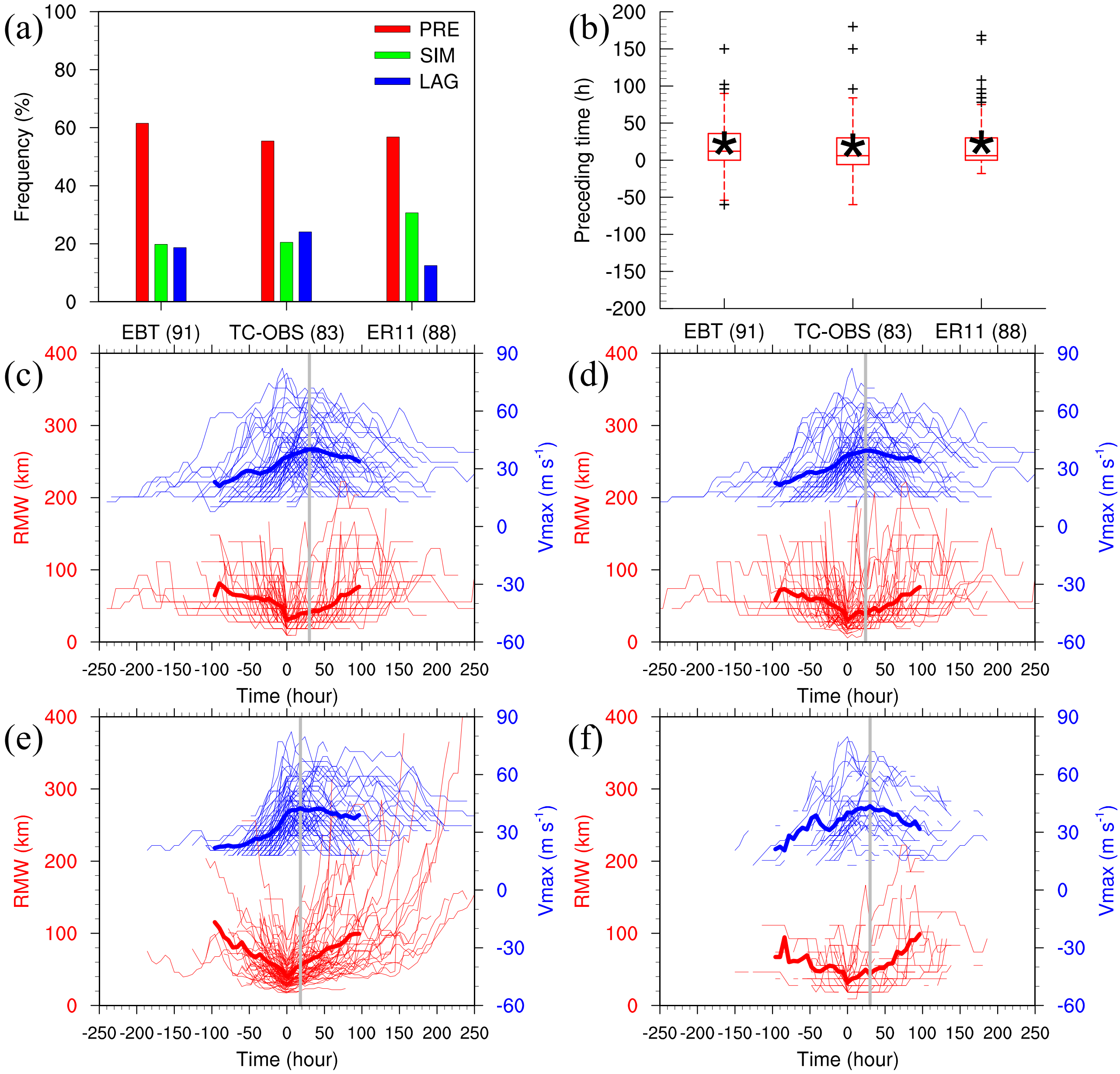

Figure 1. (a) Frequency of TCs with the end of contraction preceding (PRE), occurring simultaneously with (SIM), and lagging (LAG) the end of intensification in the NA based on EBT, TC-OBS, and ER11, respectively, with the total TC number shown in the *x*-axis label. (b) Boxplots of time difference between the ends of intensification and contraction. The bottom and top edges of each box denote the 25th and 75th percentiles and the horizontal line inside is the median. The black asterisk denotes average and the black plus sign denotes outliers. (c) Time series of RMW and TC intensity relative to the ending time of contraction based on EBT, with the results from individual TCs and composite TC shown in thin and thick curves and the end of intensification of composite result marked by grey line. (d) As in (c), but based on TC-OBS. (e) As in (c), but based on ER11. (f) As in (c), but only showing those records with aircraft observations.

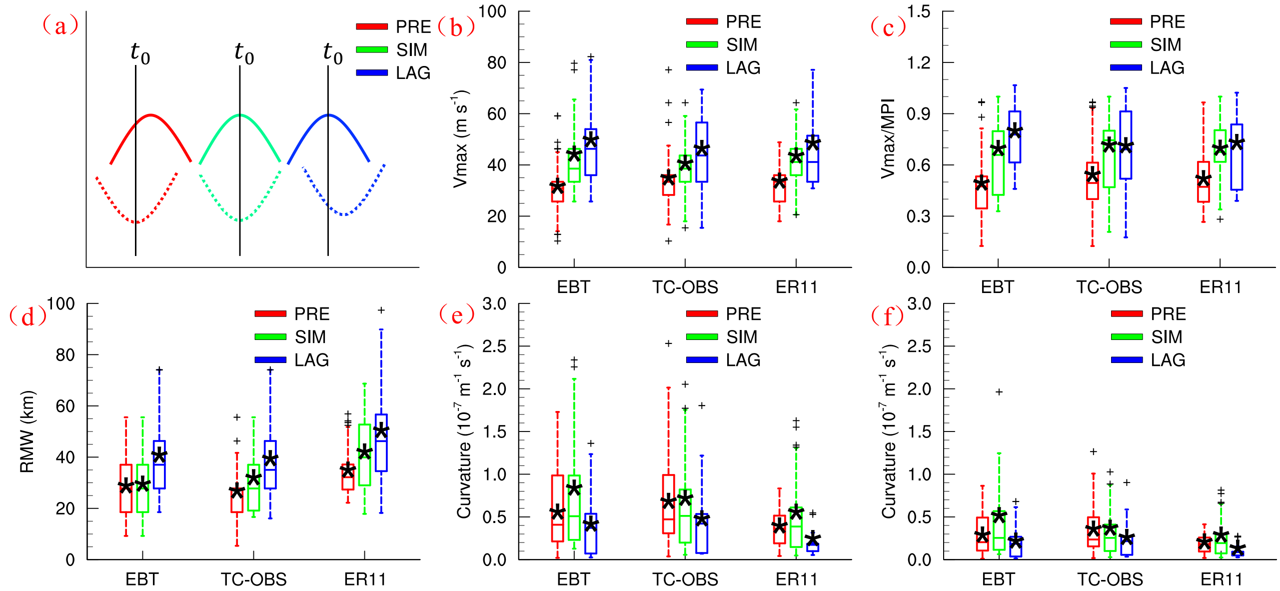

Figure 2. (a) Schematic diagram illustrating the time (t_0) used for the boxplots shown in (b)–(f), with the evolutions of TC intensity and RMW of a hypothetical TC shown in solid and dashed curves, respectively. (b) Boxplots of TC intensity at t_0 in the NA. (c) As in (b), but for the normalized TC intensity at t_0 by the average MPI between the ending times of contraction and intensification. (d) As in (b), but for RMW. (e) As in (b), but for curvature calculated by Eqs. (1) and (3) by assuming $C_k/C_D = 1$. (f) As in (e), but by assuming $C_k/C_D = 0.5$.

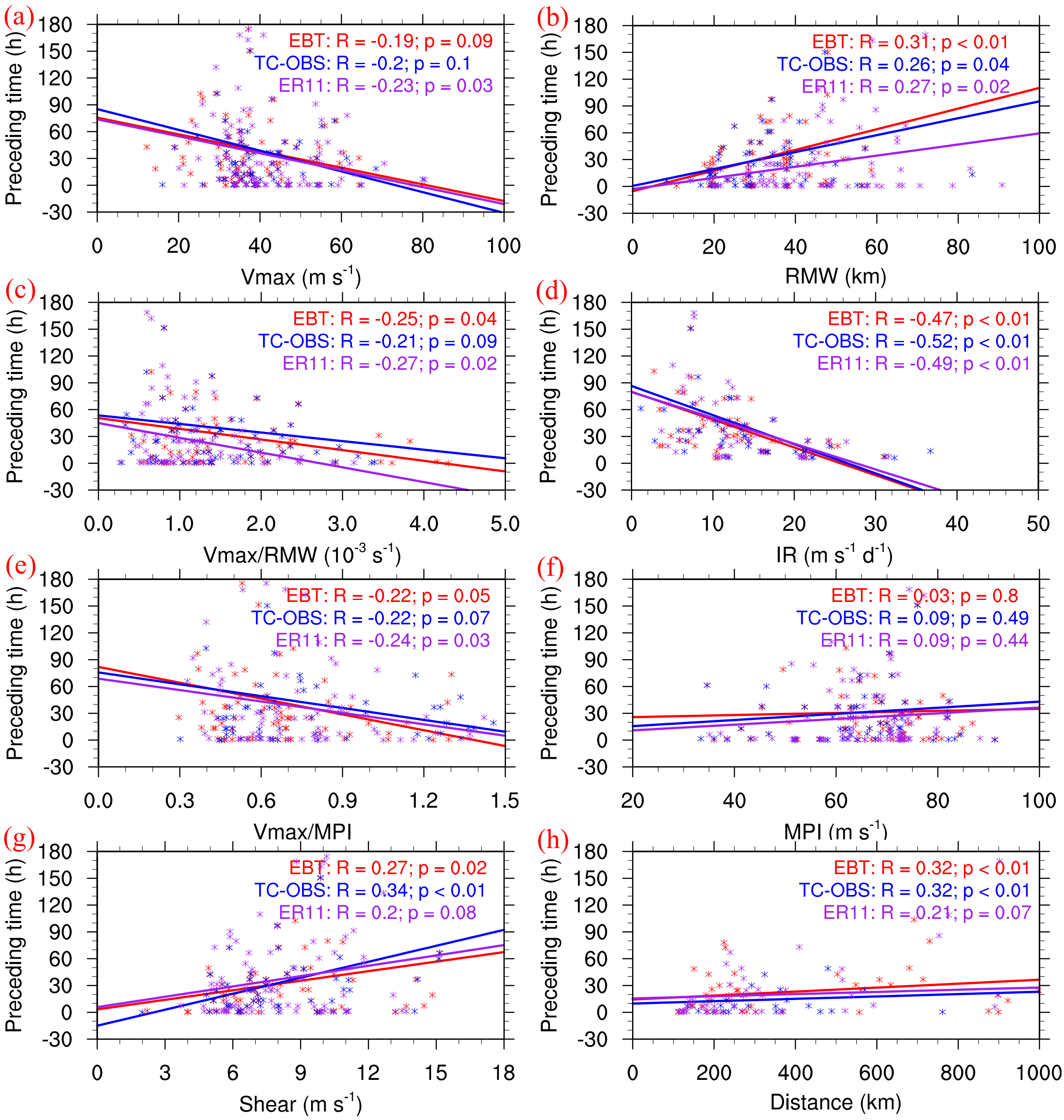

Figure 3. Scatter diagrams of the non-negative preceding time against the average (a) TC intensity, (b) RMW, (c) ratio of TC intensity to RMW, (d) intensification rate, (e) relative intensity, (f) MPI, (g) vertical wind shear, and (h) distance to the nearest major landmass between the ending times of contraction and intensification in the NA. The corresponding correlation coefficient (R) and the *p*-value as well as the linear regression line are shown in each panel.

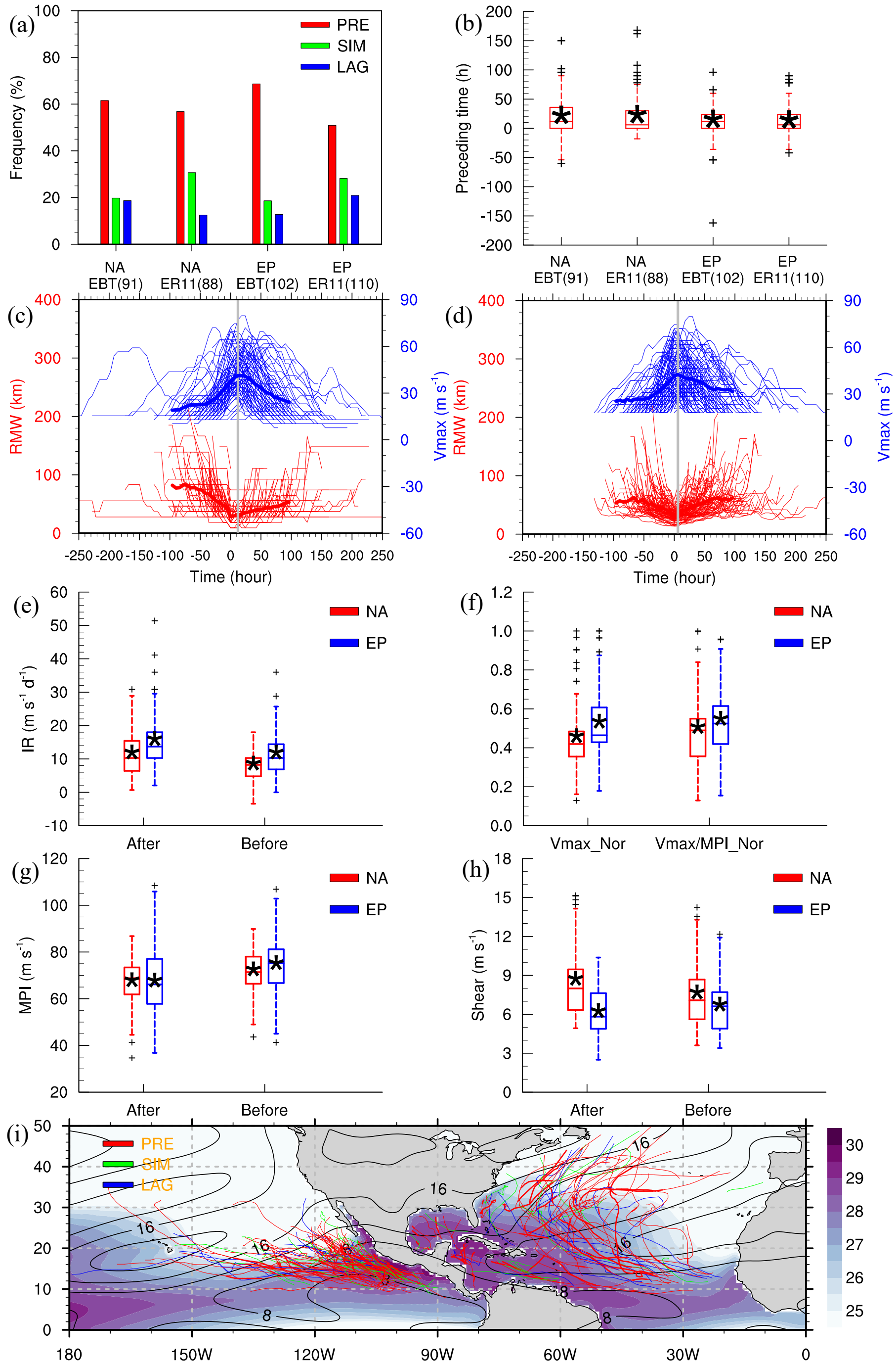

Figure 4. (a)–(b) As in Figs.1 a,b, but with results in the EP also shown. (c)–(d) As in Figs. 1c,e, but for the EP. (e) Boxplots of the average intensification rate between the ending times of contraction and intensification (“After”) and prior to the end of contraction (“Before”) for those preceding cases based on EBT. (f) Boxplots of the normalized intensity and relative intensity by the maximum values in the NA and EP at the ending time of contraction for those preceding cases based on EBT. (g) As in (e), but for MPI. (h) As in (e), but for vertical wind shear. (i) Climatological sea surface temperature (^{o}C; colored shadings) and vertical wind shear ($m\ s^{-1}$; contours) averaged during June–November (hurricane season; Supplementary Fig. S4) during 1999–2014 overlapped with tracks of all TCs, with thick red lines marking the period between the ends of contraction and intensification.